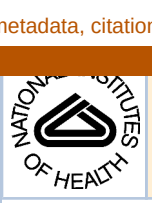

Published in final edited form as:

Arch Biochem Biophys. 2010 March 15; 495(2): 174–181. doi:10.1016/j.abb.2010.01.008.

Closure of VDAC Causes Oxidative Stress and Accelerates the Ca^{2+}-induced Mitochondrial Permeability Transition in Rat Liver Mitochondria

Andrey Tikunov[1], **C. Bryce Johnson**[1], **Peter Pediaditakis**[1,2], **Nikolai Markevich**[3], **Jeffrey M. Macdonald**[4], **John J. Lemasters**[2], and **Ekhson Holmuhamedov**[2,4,*]

[1]Department of Cell & Developmental Biology, University of North Carolina at Chapel Hill, Chapel Hill, NC 27599

[2]Center for Cell Death, Injury and Regeneration, Medical University of South Carolina, Charleston, SC 29425

[3]Department of Pathology, Anatomy & Cell Biology, Thomas Jefferson University, Philadelphia, PA 19107

[4]Department of Biomedical Engineering, University of North Carolina at Chapel Hill, Chapel Hill, NC 27599

Abstract

The electron transport chain of mitochondria is a major source of reactive oxygen species (ROS), which play a critical role in augmenting the Ca^{2+}-induced mitochondrial permeability transition (MPT). Mitochondrial release of superoxide anions ($O_2^{\bullet-}$) from the intermembrane space (IMS) to the cytosol is mediated by voltage dependent anion channels (VDAC) in the outer membrane. Here, we examined whether closure of VDAC increases intramitochondrial oxidative stress by blocking efflux of $O_2^{\bullet-}$ from the IMS and sensitizing to the Ca^{2+}-induced MPT. Treatment of isolated rat liver mitochondria with 5 μM G3139, an 18-mer phosphorothioate blocker of VDAC, accelerated onset of the MPT by 6.8 ± 1.4 min within a range of 100–250 μM Ca^{2+}. G3139-mediated acceleration of the MPT was reversed by 20 μM butylated hydroxytoluene, a water soluble antioxidant. Pre-treatment of mitochondria with G3139 also increased accumulation of $O_2^{\bullet-}$ in mitochondria, as monitored by dihydroethidium fluorescence, and permeabilization of the mitochondrial outer membrane with digitonin reversed the effect of G3139 on $O_2^{\bullet-}$ accumulation. Mathematical modeling of generation and turnover of $O_2^{\bullet-}$ within the IMS indicated that closure of VDAC produces a 1.55-fold increase in the steady-state level of mitochondrial $O_2^{\bullet-}$. In conclusion, closure of VDAC appears to impede the efflux of superoxide anions from the IMS, resulting in an increased steady-state level of $O_2^{\bullet-}$, which causes an internal oxidative stress and sensitizes mitochondria toward the Ca^{2+}-induced MPT.

*Address correspondence to: Dr. Ekhson Holmuhamedov, Center for Cell Death, Injury and Regeneration, Department of Pharmaceutical & Biomedical Sciences, Medical University of South Carolina, MSC 140, QF-309 Charleston, SC 29425, USA, Tel: 843-792-3158, Fax: 843-792-1617, holmuham@musc.edu.

Keywords

voltage dependent anion channel; mitochondria; superoxide; oxidative stress; mitochondrial permeability transition

INTRODUCTION

Mitochondria are a major source of reactive oxygen species (ROS) in mammalian cells (1–5). Superoxide anions ($O_2^{\bullet-}$) generated by the mitochondrial respiratory chain are released from both surfaces of the mitochondrial inner membrane (3,5–7). $O_2^{\bullet-}$ released into the matrix is converted to H_2O_2 by mitochondrial Mn^{2+}-dependent superoxide dismutase (SOD) (1–3,5,8, 9), and H_2O_2 so formed is further metabolized by matrix glutathione oxidoreductases, peroxiredoxins, and peroxidases, thus completing the ROS detoxification cycle (1,3,9–13). $O_2^{\bullet-}$ released into the intermembrane space (IMS) is oxidized by cytochrome *c* of the respiratory chain (1–3,5,7,11,14) or exits into the cytosol to be eliminated by cytosolic Cu^{2+}/Zn^{2+}-dependent SOD (3,8,9,13–16). Although, these reactions are sufficient to neutralize most mitochondrially generated ROS, under pathological conditions excessive generation of $O_2^{\bullet-}$ anions by Complex III can result in excess release of $O_2^{\bullet-}$ into the cytosol, oxidative stress and cell injury (2–4,6,7,15,17). Water soluble hydrophilic $O_2^{\bullet-}$ does not freely diffuse across phospholipid bilayers and most likely passes through the mitochondrial outer membrane via voltage dependent anion channels (VDAC) (18–20).

The mitochondrial permeability transition (MPT) is induced by opening of high conductance permeability transition (PT) pores in the mitochondrial inner membrane in response to excessive Ca^{2+} uptake into mitochondria (21–25). PT pore opening permeabilizes the inner membrane to solutes up to ~1500 Da and causes large amplitude mitochondrial swelling, inner membrane depolarization, and uncoupling of oxidative phosphorylation (21,22). Inducers and activators of the MPT include Ca^{2+}, inorganic phosphate, alkaline pH, phenylarsine oxide, diamide, atractyloside, mastoparan, and oxidative stress, whereas the immunosuppressive drug cyclosporin A (CsA), Mg^{2+}, low pH, and phospholipase inhibitors prevent PT pore opening and consequent mitochondrial swelling (21,22,26–28). Frequently, oxidative stress acts synergistically with other MPT inducers to promote PT pore opening (26–28).

Recently we hypothesized that alterations of mitochondrial function observed in mammalian tissues under a variety of metabolic stresses may be due to VDAC closure, which limits the normal flow of metabolites in and out of mitochondria (29,30). To further our understanding of the consequences of VDAC closure on mitochondrial functions, we investigated the effect of G3139, an 18-mer phosphorothioate oligonucleotide and recently described blocker of VDAC (29–34), on Ca^{2+}-induced PT pore opening and production of $O_2^{\bullet-}$ by isolated rat liver mitochondria. Our data are consistent with the conclusion that the closure of VDAC in respiring mitochondria impairs $O_2^{\bullet-}$ release from mitochondria, thus increasing intramitochondrial oxidative stress and accelerating onset of the MPT. Numerical simulations suggest that 80% closure of VDAC results in a 155% increase of intramitochondrial steady-state $O_2^{\bullet-}$.

MATERIALS and METHODS

Animals

All animal protocols were approved by the Institutional Animal Care and Use Committee in accordance with recommendations published in the Guide for the Care and Use of Laboratory Animals, National Academic Press, Washington DC, 1996.

Mitochondrial isolation

Rat liver mitochondria were isolated from livers of overnight-fasted male Sprague-Dawley rats (200–300 g) by differential centrifugation as described previously (35). Briefly, each liver was quickly excised, diced and homogenized in 40 ml of buffer A (0.25 M sucrose, 2 mM HEPES, 0.5 mM EGTA, pH 7.4, adjusted with KOH). The homogenate was diluted with three volumes of buffer A and centrifuged at 660 g for 15 min. The supernatant was carefully removed and centrifuged at 9700 g for 10 min. The resulting pellet was resuspended and washed twice with buffer B (0.25 M sucrose, 2 mM HEPES, pH 7.4, adjusted with KOH). Protein concentration was adjusted to 50 mg protein/ml, and mitochondria were stored on ice for further use. The mitochondrial protein was measured with a Bicinchonic Acid Protein Assay kit (Sigma, St. Louis, MO, USA) using bovine serum albumin (BSA) as standard.

Mitochondrial swelling

Isolated rat liver mitochondria (1 mg/ml) were suspended in mitochondrial incubation buffer (MIB) containing 200 mM sucrose, 5 mM succinate, 2 μM rotenone, 1 μg/ml oligomycin, 1 mM KH_2PO_4, 20 μM EGTA, 20 mM Tris/HEPES buffer, pH 7.4 and incubated 5 min at room temperature (RT) with or without modifiers. Mitochondrial suspensions were then aliquoted into 96-well clear microtiter plates (0.2 ml/well) and exposed to different Ca^{2+} concentrations (0, 100, 150, 200, 250 and 300 μM). Absorbance at 544 nm was monitored using a FLUOStar multi-well plate reader (BMG Labtech, Durham, NC, USA).

$O_2^{\bullet-}$ measurement

Isolated rat liver mitochondria (1 mg/ml) were suspended in MIB, incubated with and without modifiers for 4 min at RT, and then treated with 2 μM dihydroethidium (DHE) (Invitrogen, Eugene, OR, USA). After addition of DHE, mitochondria were incubated for another 1 min and then added to microtiter plates containing the respiratory inhibitor antimycin A (1 μg/ml) to promote $O_2^{\bullet-}$ production at Complex III (5–7). $O_2^{\bullet-}$ formation was inferred from increased red fluorescence of ethidium (oxidized DHE) measured with excitation and emission wavelengths of 485 nm and 610 nm, respectively (7). White 96-well microtiter plates were used to maximize the sensitivity of the assay and prevent loss of fluorescent light through transparent walls. The rate of $O_2^{\bullet-}$ production was expressed as relative fluorescent units (RFU)/min/mg protein.

Distribution of ethidium in mitochondrial suspensions

Isolated rat liver mitochondria (1 mg/ml) were suspended in MIB and pre-treated with DHE (2 μM) for 1 min at RT. Subsequently, antimycin A (1 μg/ml) was added, and mitochondria were incubated for another 5 min at RT. After incubation, mitochondria were separated from buffer by rapid centrifugation in a microfuge (14,000 rpm for 60 s). Supernatants were saved, and mitochondrial pellets were resuspended in the initial volume of incubation buffer. Ethidium fluorescence in supernatants and mitochondria was measured using white 96-well plates in the fluorescence plate reader.

Mitochondrial outer membrane permeability

Isolated rat liver mitochondria (1 mg/ml) were suspended in MIB and pre-incubated with and without modifiers for 5 min at RT. An aliquot of the suspension (500 μl) was quickly mixed with calcein (40 μM) and layered over the 100 μl of silicone oil placed into a 1.5 ml Eppendorf tube as described (36). The density of silicone oil was adjusted to 1.03 g/ml by mixing equal volumes of two silicone oils with density 1.01 g/ml and 1.05 g/ml (Sigma, Cat # 10836 & Cat # 175633). Immediately after layering the mitochondrial suspensions, the tubes were centrifuged at 14,000 rpm for 60 s in an Eppendorf MiniSpin microcentrifuge (Eppendorf, Westbury, NY) to sediment mitochondria into the silicone oil. After centrifugation, the upper

aqueous layer was aspirated, and the walls of the Eppendorf tube were rinsed with incubation buffer 3 times, leaving the mitochondrial pellet and oil layer undisturbed. The oil layer was then aspirated, and the mitochondrial pellet was resuspended in 500 µl 0.1 % Triton X100, sonicated for 30 s (Branson, Danbury, CT) and vortexed. The remaining silicone oil droplets were removed by centrifugation (14,000 rpm for 60 s). Calcein fluorescence in the supernatant was measured using white 96-well microtiter plates and excitation and emission wavelengths of 495 nm and 520 nm, respectively.

Mitochondrial respiration

Oxygen consumption by isolated mitochondria was measured in MIB, using a Clark style oxygen electrode, as described (29). Respiration was expressed as nmol O_2/min/mg protein.

Materials

G3139 was a generous gift from Dr. Robert Brown (Genta, Inc, Berkeley Heights, NJ, USA). Unless otherwise stated, all chemicals used in this study were obtained from Sigma (St. Louis, MO, USA).

Statistics

Differences between groups were analyzed by 2-way ANOVA using $p<0.05$ as the criterion of significance. Results were expressed as means ± S.E.M.. When error bars are not seen on the graphs, they fall within the diameters of the symbols. Images are representative of at least 3 experiments.

RESULTS

Dose-dependence of the Ca^{2+}-induced MPT

Typical absorbance changes of mitochondrial suspensions due to onset of the MPT after treatment with different doses of Ca^{2+} are shown in Fig. 1A. In the absence of Ca^{2+}, swelling (decrease of absorbance) did not occur during the 45 min time of observation (Fig. 1A, curve “a”, *open circles*). Increasing amounts of Ca^{2+} led to onset of swelling (MPT) at progressively earlier time points, as manifested by decreasing absorbance after Ca^{2+} (Fig. 1A, curves “a” through “f”,). The uniformity of the absorbance curves obtained for different concentrations of added Ca^{2+} (Fig. 1A, curves “a”-”f”) and reproducibility of the maximal and minimal levels of absorbance (Fig. 1A, dotted lines A_{max} & A_{min}) allowed quantitative comparison of MPT between different samples. The time ($\boldsymbol{T}_{50\%}$) to a 50% decrease of absorbance (A1/2) served as a measure of the sensitivity of mitochondria to the Ca^{2+}-induced MPT (Fig. 1B). CsA (1 µM), a PT pore inhibitor (37), blocked swelling at all concentrations of Ca^{2+} used, which confirmed that swelling was due to opening of PT pores (Fig. 1A, curve “g”, *filled triangles*).

Effect of G3139 treatment on the Ca^{2+}-induced MPT

Pretreatment of mitochondria with 5 µM G3139, a VDAC blocker (32–34), for 5 min accelerated onset of the Ca^{2+}-induced MPT and decreased $T_{50\%}$ for swelling, although in the absence of Ca^{2+}, G3139 did not cause swelling (Fig. 2). On average, G3139 decreased $T_{50\%}$ by 6.8 ± 1.4 min over the entire range of Ca^{2+} concentrations used (Fig. 2B). This decrease of $T_{50\%}$ was equivalent to the decrease produced by increasing Ca^{2+} by 44 ± 5 µM Ca^{2+} (Fig. 2B). In the presence of G3139, CsA nonetheless retained its ability to inhibit Ca^{2+}-induced mitochondrial swelling (Fig. 2A, curve a), confirming that mitochondrial swelling in the presence of G3139 was due to PT pore opening.

Reversal by Butylated Hydroxytoluene of G3139-accelerated Mitochondrial Swelling

Oxidative stress sensitizes mitochondria to the Ca^{2+}-induced MPT (28,38–40). In accordance, butylated hydroxytoluene (BHT, 20 μM), an antioxidant, delayed Ca^{2+}-induced mitochondrial swelling 8.7 ± 0.5 min (Fig. 3A, compare *open* and *closed circles*, curves c and b). This increase of $\boldsymbol{T}_{50\%}$ was equivalent to decreasing added Ca^{2+} by 60 ± 15 μM (Fig. 3A, compare *open* and *closed circles*, curves c and b). The acceleration of MPT onset and decrease of $\boldsymbol{T}_{50\%}$ by G3139 was reversed by BHT (20 μM) added before induction of the MPT with Ca^{2+} (Fig. 3A, compare curves a and d). The delay of MPT onset by BHT (20 μM) occurred for entire range of Ca^{2+} concentrations studied (Fig. 3B, compare curves c and b). Similarly, BHT reversed the effect of G3139 at all Ca^{2+} concentrations studied (Fig. 3B, curves a and d, *open triangles* & *open squares*, respectively).

Measurements of $O_2^{\bullet-}$ in mitochondria

We further tested the effect of G3139 on mitochondrial $O_2^{\bullet-}$ production after antimycin A (1 μg/ml) treatment using DHE, a membrane permeable probe that reacts with $O_2^{\bullet-}$ to form the highly fluorescent ethidium cation (5–7). Rates of increase of ethidium fluorescence after antimycin A were determined in control and G3139-treated mitochondria oxidizing succinate in the presence and absence of added SOD. Antimycin A, an inhibitor of Complex III, was used to increase mitochondrial $O_2^{\bullet-}$ production (5–7). G3139 (5 μM) increased antimycin A-stimulated $O_2^{\bullet-}$ measured by DHE from 34.8 ± 2.5 to 54.2 ± 3.8 RFU/min/mg protein, indicating a 55 ± 6% increase (Fig. 4, **None** and **G3139**). In both the presence and absence of G3139, $O_2^{\bullet-}$ formation was not affected by SOD added to incubation media (Fig. 4, **SOD**), indicating that the compartment forming $O_2^{\bullet-}$ and reacting with DHE was not accessible to extramitochondrial SOD. Rapid separation of mitochondria from the incubation buffer by microcentrifugation showed that ~95% of total ethidium fluorescence was associated with mitochondria with the remainder in the supernatant (data not shown). Thus, ethidium fluorescence was primarily reflecting $O_2^{\bullet-}$ formation within mitochondria.

Measurement of mitochondrial outer membrane permeability

To measure permeability of the mitochondrial outer membrane directly, we adopted a method of rapid centrifugation of mitochondria through a layer of silicone oil, allowing fast separation of mitochondria from the calcein-containing incubation buffer (36). During centrifugation, mitochondria passing through silicone layer are stripped of their surrounding medium, but calcein within the intermembrane space sediments with the mitochondria. In the absence of G3139, calcein fluorescence associated with mitochondria was 22.6 ± 0.7 RFU/mg protein (Fig. 5, **None**). When mitochondria were pre-treated with G3139 (5 μM), calcein fluorescence associated with the sedimented mitochondria became 15.2 ± 0.6 RFU/mg protein, a decrease of 35 ± 5% (Fig. 5, **G3139**). Digitonin (50 μM) pretreatment of mitochondria to permeabilize the outer membrane (29,30,41,42) partially reversed this effect of G3139, but in the absence of G3139 did not alter calcein retention (Fig. 5, **Digitonin**). These observations are consistent with conclusion that G3139 decreases the permeability of the outer membrane to calcein, consistent with inhibition of VDAC conductance.

Effect of G3139 treatment on the activity of Ca^{2+}-uniporter

Treatment of isolated mitochondria with G3139 may interfere with Ca^{2+} uptake into mitochondria and thus alter onset of the Ca^{2+}-induced MPT. To initiate the MPT, respiration-driven Ca^{2+} uptake must occur via the Ca^{2+} uniporter, and the rate of Ca^{2+}-activated respiration is a measure of the rate of mitochondrial Ca^{2+} uptake (25) . To assess the effect of G3139 on the rate of Ca^{2+} uptake in mitochondria, we measured the initial rate of Ca^{2+}-activated mitochondrial respiration in the same medium used for swelling experiments (see Fig. 1–Fig. 3). Addition of Ca^{2+} (250 μM) to untreated mitochondria, increased respiration from 7.2 ± 0.2

to 52.2 ± 2.6 nmol O_2/min/mg protein, a 7-fold increase (Fig. 6, **None**). In the presence of G3139, the initial rate of Ca^{2+}-stimulated respiration increased from 5.5 ± 0.4 to 46.3 ± 1.0 nmol O_2/min/mg protein, relative 8-fold increase, although the absolute rate of Ca^{2+}-activated respiration decreased by 11% (Fig. 6, **G3139**). These small differences in the rate of Ca^{2+} uptake into the mitochondria cannot account for the several minute delay of MPT onset by G3139.

Mathematical model of superoxide metabolism in the mitochondrial intermembrane space

To estimate how the open-closed status of VDAC could affect steady state $O_2^{\bullet-}$ in the mitochondrial intermembrane space, we developed a mathematical model, which is based on our own and available experimental data. The mathematical model describes the steady state level of $O_2^{\bullet-}$ within the intermembrane space (IMS) of mitochondria with open and closed VDAC. Our model includes the following 4 processes of generation and annihilation of $O_2^{\bullet-}$ within the IMS of mitochondria (Fig. 7):

1. Generation of $O_2^{\bullet-}$ by Complex III of the respiratory chain—The rate of change of $O_2^{\bullet-}$ concentration in the IMS produced by Complex III (J_{RC}) may be described as follows (43):

$$J_{RC}=(V_{mito}/V_{IMS})\times k_{bc1}\times[bc1] \quad (1)$$

where: k_{bc1} is the rate constant for superoxide generation by isolated antimycin A-treated cytochrome *bc*$_1$ (Complex III) (3); [bc1] is the concentration of cytochrome *bc*$_1$(Fig. 7, Complex III) in the mitochondrial inner membrane normalized to the total mitochondrial protein (3,44), and V_{mito}/V_{IMS} is the inverse fractional ratio of IMS of the total mitochondrial volume.

The relationship between mitochondrial matrix volume (V_{mito}) and the volume of IMS (V_{IMS}) is determined by mitochondrial energetic status of and the tonicity of the incubation buffer (45–47). Under our experimental conditions, we expect mitochondria to be in a condensed configuration, and we assume that the IMS will represent one-half of the total mitochondrial volume (45,46). Substitution of known parameters of mitochondria (Table 1) into equation (1) produces a simplified equation describing changes of $O_2^{\bullet-}$ concentration within the mitochondrial IMS:

$$J_{RC}=80\,\mu M/s \quad (2)$$

2. $O_2^{\bullet-}$ dismutation—The IMS contains a negligible content of active SOD (4,8). Accordingly in our model, we assume that only spontaneous non-enzymatic dismutation of $O_2^{\bullet-}$ occurs (48):

$$2O_2^{\bullet-}+2H^+ \overset{k_{dis}}{\Longleftrightarrow} O_2+H_2O_2 \quad (3)$$

The overall flux of superoxide dismutation at neutral pH can be expressed as (8):

$$J_{Dis}=k_{dis}[O_2^{\bullet-}]^2 \quad (4)$$

where: J_{dis} is the flux of superoxide anion dismutation, k_{dis} is the second order rate constant for superoxide dismutation, measured in $\mu M^{-1}s^{-1}$, and $[O_2^{\bullet-}]$ is $O_2^{\bullet-}$ concentration.

3. Oxidation of $O_2^{\bullet-}$ by cytochrome *c* within the mitochondrial IMS—$O_2^{\bullet-}$ released into the IMS reacts with oxidized cytochrome *c* producing molecular oxygen and reduced cytochrome *c* (1,2,14):

$$O_2^{\bullet-} + \text{cyt c}(Fe^{3+}) \underset{k_{-cyt\ c}}{\overset{k_{cyt\ c}}{\Longleftrightarrow}} O_2 + \text{cyt c}(Fe^{2+}) \quad (5)$$

The equilibrium constant of this redox reaction can be expressed as $K_{eq} = k_{cyt\ c}/k_{-cyt\ c} = \exp(\Delta E_m \cdot n \cdot F/R \cdot T)$, where K_{eq} is the equilibrium constant, $k_{cyt\ c}$ and $k_{-cyt\ c}$ are the forward and reverse rate constants, ΔE_m is the difference of the midpoint potentials of the redox pairs participating in the reaction, F is the Faraday's constant, R is the gas constant, T is the absolute temperature and n is the number of electrons transferred. To calculate the contribution of cytochrome *c* mediated oxidation of $O_2^{\bullet-}$ in reaction (5), we used values of the midpoint potentials for the pairs of cyt c(Fe^{3+})/cyt c(Fe^{2+}) and O_2/ $O_2^{\bullet-}$ determined in (49) and shown in Table 1. The absolute values of midpoint potentials indicate that oxidized cytochrome c is a strong oxidant and will act as an acceptor with high affinity for electrons and that $O_2^{\bullet}$ is strong reducing agent with high capacity to donate electrons to oxidized cytochrome *c*. The corresponding value of the equilibrium constant for reaction (5) calculated from these data ($K_{eq} \sim 1.3 \cdot 10^7$) indicates the reaction is highly irreversible in the forward direction, allowing simplification of the rate reaction to (5).

$$J_{cyt\ c} = k_{cyt\ c} \times [O_2^{\bullet-}] \times \left[\text{cyt c}(Fe^{3+})\right] \quad (6)$$

where: $J_{cyt\ c}$ is the flux of $O_2^{\bullet-}$, $k_{cyt\ c}$ is the forward rate constant, $[O_2^{\bullet-}]$ is the concentration of $O_2^{\bullet}$, and [cyt c (Fe^{3+})] is the concentration of oxidized cytochrome *c*. After reduction in the IMS, reduced cytochrome *c* is rapidly re-oxidized by cytochrome *c* oxidase. Since cytochrome *c* oxidase activity is so much greater that cytochrome *c* reduction by antimycin-inhibited cytochrome bc_1, virtually all cytochrome *c* remains in the oxidized state (50–52). Taking into account the total concentration of cytochrome *c* in the IMS of liver mitochondria (44) we estimated that the concentration of oxidized cyt c (Fe^{3+}) approximates 700 μM, the value used in our model in equation (6).

4. Efflux of $O_2^{\bullet-}$ through VDAC—The last process in $O_2^{\bullet-}$ metabolism is efflux of $O_2^{\bullet-}$ through VDAC (J_{VDAC}), which can be described as follows:

$$J_{VDAC} = P_{VDAC} \times [O_2^{\bullet-}] \quad (7)$$

where: P_{VDAC} (measured in s^{-1}) is the permeability of VDAC for $O_2^{\bullet-}$. The value of P_{VDAC} in intact mitochondria is unknown, and in our modeling we assume that G3139 at the doses used in our work will induce an approximately 80% decrease in the conductance of VDAC, in accord with recent observations (33,34).

Computational results

At steady state, the rate of change of $O_2^{\bullet-}$ concentration within the IMS is described by the following equation:

$$d[O_2^{\bullet -}]/dt = J_{RC} - J_{Dis} - J_{VDAC} - J_{cyt\ c} = 0 \quad (8)$$

Substitution of fluxes and values of parameters (Table 1) into equation (8) allows derivation of an expression for the steady state concentration of $O_2^{\bullet -}$ (in μM) as a function of VDAC permeability (P_{VDAC})::

$$[O_2^{\bullet -}] = -(700+P_{VDAC})/1.2 + \left(\sqrt{(700+P_{VDAC})^2+192}\right)/1.2 \quad (9)$$

Numerical computations based on equation (9) produce a dependence of steady-state $O_2^{\bullet -}$ concentration in the IMS on the VDAC permeability as shown in Fig. 8 (*dotted* line). The solid portion of the curve (Fig. 8, *solid* line) shows that $O_2^{\bullet -}$ concentration within the IMS increases from 0.0635 to 0.0985 μM when the permeability of VDAC (P_{VDAC}) decreases by 80%, from 560 s^{-1} to 112 s^{-1}.

DISCUSSION

Opening of mitochondrial PT pores initiates onset of the mitochondrial permeability transition (MPT) with consequent mitochondrial depolarization, uncoupling of oxidative phosphorylation and large amplitude mitochondrial swelling. Calcium, inorganic phosphate, alkaline pH, oxidative stress and various oxidant chemicals promote PT pore opening, whereas as cyclosporin A and pH less than 7 inhibit pore opening (21,22,26–28,40). The molecular identity of the pore remains unresolved and controversial. In one model, the PT pore is a complex of the adenine nucleotide transporter (ANT) from the inner membrane, cyclophilin D (CypD) from the matrix and VDAC from the outer membrane. In this model, VDAC forms part of the solute-conducting channel of the PT pore. Accordingly, we evaluated whether inhibition of VDAC channel conductance with G3139, an 18-mer phosphorothioate polyoligonucleotide inhibitior of mitochondrial VDAC (32–34,53), would block or delay PT pore opening and onset of the MPT. However, contrary to expectation, G3139 accelerated onset of the Ca^{2+}-induced MPT, as manifested by a shortening of the time to half maximal swelling ($\mathbf{T_{50\%}}$) (Fig. 2). This acceleration of the Ca^{2+}-induced MPT onset occurred at all Ca^{2+} concentrations examined. This result suggests that VDAC does not form part of the solute-conducting channel of PT pores and is consistent with recent findings that the MPT still occurs in mitochondria deficient of VDAC isoforms (54)

Although G3139 accelerated rather than blocked MPT onset, the polyoligonucleotide nonetheless decreased permeability of the outer membrane to hydrophilic solutes as assessed by rapid sedimentation through silicone oil. Centrifugal sedimentation separates individual mitochondria from the bulk medium, except for an aqueous shell surrounding each mitochondrion (36). Using calcein, a water soluble fluorophore that crosses the outer but not the inner membrane through VDAC into the IMS, we showed that G3139 decreased the amount of calcein sedimenting with mitochondria through silicone in a fashion that was largely reversed by outer membrane disruption with digitonin (Fig. 5). These results show that G3139 blocks access of calcein to a space opened by digitonin, namely the IMS. Since access to the IMS is provided by VDAC, we can conclude that G3139 does indeed inhibit VDAC in our isolated rat liver mitochondria, as shown previously for VDAC in reconstituted bilayers (31, 33,34,53). Digitonin, however, did not completely restore the initial level of calcein sedimenting with mitochondria through silicone oil (Fig. 5). Digitonin causes vesiculation of the outer membrane (41,44). Some of these vesicles remain attached to mitochondria. In the

presence of G3139, these vesicles may exclude calcein, which would explain the lack of full recovery of calcein sedimentation.

Mitochondrial Ca^{2+} uptake, the initiating factor for onset of the MPT, might also be affected by VDAC closure. To assess this possibility, we estimated rates of mitochondrial Ca^{2+} uptake from rates of Ca^{2+}-stimulated respiration. G3139 decreased Ca^{2+} -induced respiration by only 11% (Fig. 6, **Ca^{2+}/G3139**). This small G3139-induced decrease of the rate of Ca^{2+} uptake might slightly delay MPT onset, but to the contrary G3139 accelerated MPT onset. Thus, effects on Ca^{2+} uptake do not explain G3139-dependent acceleration of MPT onset.

The mitochondrial electron transport chain is a major source of intracellular ROS, including $O_2^{\bullet-}$(1,2,5,6). Normally, the respiratory chain releases $O_2^{\bullet-}$ from both sides of the inner membrane, namely to the matrix and the IMS. In the matrix, mitochondrial superoxide dismutase, catalase, glutathione peroxidases and peroxiredoxins detoxify $O_2^{\bullet-}$ and H_2O_2 (1, 3,4,7,9,11,20). For $O_2^{\bullet-}$ released into the IMS, $O_2^{\bullet-}$ is principally detoxified via oxidation by cytochrome *c* or by cytosolic SOD after release into the cytosol. $O_2^{\bullet-}$ is hydrophilic and negatively charged and therefore must cross the outer membrane via VDAC (18–20). Accordingly, VDAC may be an important regulator of $O_2^{\bullet-}$ diffusion from the IMS to the cytosol (19), and $O_2^{\bullet-}$ retention after VDAC closure may cause intramitochondrial oxidative stress and promote onset of the MPT while simultaneously protecting the cytosol against oxidative stress (30).

To test the hypothesis that increased oxidative stress after VDAC closure with G3139 was accelerating the MPT, we evaluated the effect of the antioxidant, BHT, on the G3139-accelerated MPT onset. In the absence of G31239 or BHT, Ca^{2+} induced characteristic S-shaped mitochondrial swelling as monitored by absorbance of mitochondrial suspensions (Fig. 1A) and expressed as the time required for a 50% change ($\mathbf{T_{50\%}}$) to occur (Fig. 2B). As Ca^{2+} increased, $\mathbf{T_{50\%}}$ decreased. G3139 further accelerated MPT onset to extent comparable to that after increasing added Ca^{2+} by 44 ± 5 μM The antioxidant, BHT, reversed acceleration of the MPT by G3139 and also delayed the MPT in the absence of G3139 (Fig. 3). Consistent with earlier studies (17,28), these results suggested that ROS are involved in onset of the Ca^{2+}-induced MPT.

To address directly the effect of G3139 on mitochondrial ROS generation, we measured $O_2^{\bullet-}$ production using DHE. Nonfluorescent DHE reacts with $O_2^{\bullet-}$ to form red-fluorescing ethidium (55–57). To enhance $O_2^{\bullet-}$ formation, mitochondria were treated with antimycin in the presence of succinate and rotenone. Under these conditions, $O_2^{\bullet-}$ is principally released by Complex III into the IMS. (1,3,6,7). After release of $O_2^{\bullet-}$ into the extramitochondrial space, $O_2^{\bullet-}$ becomes diluted by more than a 1000-fold and is further decreased by spontaneous dismutation. Accordingly, ethidium generation predominantly occurs within the IMS where modeling indicates that $O_2^{\bullet-}$ concentration is 0.5–2 μM or near the surface of mitochondria where local $O_2^{\bullet-}$ concentrations are highest. This interpretation is supported by the observation that exogenous SOD, an enzyme that degrades $O_2^{\bullet-}$ in the extramitochondrial space, did not alter generation of ethidium fluorescence (Fig. 4) In antimycin-treated mitochondria, G3139 increased the rate of ethidium formation by 75±7%, which was reversed by outer membrane permeabilization with digitonin (Fig. 4). These results are consistent with the conclusion that G3139 by blocking VDAC causes an increase of $O_2^{\bullet-}$ in the IMS. However, closure of VDAC by itself was not sufficient to initiate the MPT in isolated mitochondria and required increased Ca^{2+} loading. Ca^{2+} may have the dual role of both opening PT pores in a CypD-dependent fashion and of promoting mitochondrial ROS generation (1,22,26,27,58).

Mathematical modeling was used to assess the expected effect of VDAC closure on $O_2^{\bullet-}$ levels in the IMS. According to the model, steady-state [$O_2^{\bullet-}$] increases exponentially with

progressive closure of VDAC. For the reported maximal 80% closure of reconstituted VDAC by G3139 (33,34,53,59), VDAC permeability changes from 560 s^{-1} to 112 s^{-1}, leading to 55% increase in [$O_2^{\bullet}$] after G3139, in good agreement with our experimental findings (Fig. 4). After 100% VDAC closure (P_{VDAC} = 0 s^{-1}), the mathematical model predicts a 2.4-fold increase of [$O_2^{\bullet-}$] from 0.047 to 0.114 μM $O_2^{\bullet-}$ does not increase above this concentration because of oxidation by cytochrome *c* and spontaneous dismutation.

In conclusion, opening and closing of the VDAC pathways may be important to regulate both intramitochondrial $O_2^{\bullet-}$ levels and the release of $O_2^{\bullet-}$ from mitochondrial into the cytosol. Although ROS can induce cell injury, increasing evidence indicates a role for ROS as a vital intracellular signal (1–5). Thus, VDAC may regulate release of ROS signals in normal cellular physiology (1,4,5,13). In this way, opening and closure of VDAC can provide a simple and flexible mechanism of transduction of extracellular stress signals into the cytosol for the purposes of metabolic control. By contrast in pathophysiological settings, VDAC closing may spare oxidative stress in the cytosol while promoting intramitochondrial oxidative stress by decreasing mitochondrial release of $O_2^{\bullet-}$. In particular, intramitochondrial oxidative stress from VDAC closure sensitizes mitochondria to the MPT and may cause downstream activation of pathways to apoptotic and necrotic cell death.

Abbreviations used

BHT	butylated hydroxytoluene
CsA	cyclosporin A
DHE	dihydroethidium
CypD	cyclophilin D
IMS	intermembrane space
MIB	mitochondrial incubation buffer
MOM	mitochondrial outer membrane
MPT	mitochondrial permeability transition
$O_2^{\bullet-}$	superoxide anion
PT	permeability transition
RFU	relative fluorescence unit
ROS	reactive oxygen species
RT	room temperature
SOD	superoxide dismutase
VDAC	voltage dependent anion channel.

Acknowledgments

This work was supported, in part, by Grants AA016011, K25 AA016604, DK37034 and DK073336 from the National Institutes of Health and a Pilot Feasibility Grant from the Center of Gastrointestinal Biology and Disease, University of North Carolina at Chapel Hill, Chapel Hill, NC USA.

Reference List

1. Andreyev A, Yu, Kushnareva YE, Starkov AA. Biochemistry, (Moscow) 2005;20:200–214. [PubMed: 15807660]

2. Cadenas E, Davies KJ. Free Radic. Biol. Med 2000;29:222–230. [PubMed: 11035250]
3. Drose S, Brandt U. J Biol. Chem 2008;283:21649–21654. [PubMed: 18522938]
4. Inarrea P, Moini H, Han D, Rettori D, Aguilo I, Alava MA, Iturralde M, Cadenas E. Biochem. J 2007;405:173–179. [PubMed: 17394422]
5. Turrens JF. Biosci. Rep 1997;17:3–8. [PubMed: 9171915]
6. Han D, Williams E, Cadenas E. Biochem. J 2001;353:411–416. [PubMed: 11139407]
7. Piskernik C, Haindl S, Behling T, Gerald Z, Kehrer I, Redl H, Kozlov AV. Biochim. Biophys. Acta 2008;1782:280–285. [PubMed: 18298959]
8. Okado-Matsumoto A, Fridovich I. J Biol. Chem 2001;276:38388–38393. [PubMed: 11507097]
9. Weisiger RA, Fridovich I. J Biol. Chem 1973;248:4793–4796. [PubMed: 4578091]
10. Antunes F, Han D, Cadenas E. Free Radic. Biol. Med 2002;33:1260–1267. [PubMed: 12398934]
11. Cao Z, Lindsay JG, Isaacs NW. Subcell. Biochem 2007;44:295–315. [PubMed: 18084900]
12. Handy DE, Lubos E, Yang Y, Galbraith JD, Kelly N, Zhang YY, Leopold JA, Loscalzo J. J Biol. Chem 2009;284:11913–11921. [PubMed: 19254950]
13. Jezek P, Hlavata L. Int. J Biochem. Cell Biol 2005;37:2478–2503. [PubMed: 16103002]
14. Lambert AJ, Brand MD. Methods Mol. Biol 2009;554:165–181. [PubMed: 19513674]
15. Brand MD, Affourtit C, Esteves TC, Green K, Lambert AJ, Miwa S, Pakay JL, Parker N. Free Radic. Biol. Med 2004;37:755–767. [PubMed: 15304252]
16. Goldsteins G, Keksa-Goldsteine V, Ahtoniemi T, Jaronen M, Arens E, Akerman K, Chan PH, Koistinaho J. J Biol. Chem 2008;283:8446–8452. [PubMed: 18171673]
17. Dawson TL, Gores GJ, Nieminen AL, Herman B, Lemasters JJ. Am. J. Physiol 1993;264:C961–C967. [PubMed: 8386454]
18. Madesh M, Hajnoczky G. J Cell Biol 2001;155:1003–1015. [PubMed: 11739410]
19. Han D, Antunes F, Canali R, Rettori D, Cadenas E. J Biol. Chem 2003;278:5557–5563. [PubMed: 12482755]
20. Karachitos A, Galganska H, Wojtkowska M, Budzinska M, Stobienia O, Bartosz G, Kmita H. FEBS Lett 2009;583:449–455. [PubMed: 19116152]
21. Bernardi P, Forte M. Novartis. Found. Symp 2007;287:157–164. [PubMed: 18074637]
22. Crompton M, Virji S, Doyle V, Johnson N, Ward JM. Biochem. Soc. Symp 1999;66:167–179. [PubMed: 10989666]
23. Haworth RA, Hunter DR. Arch. Biochem. Biophys 1979;195:460–467. [PubMed: 38751]
24. Hunter DR, Haworth RA. Arch. Biochem. Biophys 1979;195:468–477. [PubMed: 112926]
25. Gunter TE, Pfeiffer DR. Am. J. Physiol 1990;258:C755–C786. [PubMed: 2185657]
26. Halestrap AP. Biochem. Soc. Trans 2006;34:232–237. [PubMed: 16545083]
27. Lemasters JJ. Cardiovasc Res 1999;44:470–473. [PubMed: 10690277]
28. Nieminen AL, Byrne AM, Herman B, Lemasters JJ. Am J Physiol 1997;272:C1286–C1294. [PubMed: 9142854]
29. Holmuhamedov E, Lemasters JJ. Arch. Biochem. Biophys 2009;481:226–233. [PubMed: 19014900]
30. Lemasters JJ, Holmuhamedov E. Biochim. Biophys. Acta 2006;1762:181–190. [PubMed: 16307870]
31. Colombini M. Mol Cell Biochem 2004;256–257:107–115.
32. Lai JC, Tan W, Benimetskaya L, Miller P, Colombini M, Stein CA. Proc. Natl. Acad. Sci. U. S. A 2006;103:7494–7499. [PubMed: 16648253]
33. Tan W, Loke YH, Stein CA, Miller P, Colombini M. Biophys. J 2007;93:1184–1191. [PubMed: 17483171]
34. Tan W, Lai JC, Miller P, Stein CA, Colombini M. Am J Physiol Cell Physiol 2007;292:C1388–C1397. [PubMed: 17135295]
35. Lemasters JJ, Grunwald R, Emaus RK. J. Biol. Chem 1984;259:3058–3063. [PubMed: 6321493]
36. Hoek JB, Coll KE, Williamson JR. J Biol. Chem 1983;258:54–58. [PubMed: 6129254]
37. Broekemeier KM, Dempsey ME, Pfeiffer DR. J Biol. Chem 1989;264:7826–7830. [PubMed: 2470734]

38. Kanno T, Sato EE, Muranaka S, Fujita H, Fujiwara T, Utsumi T, Inoue M, Utsumi K. Free Radic. Res 2004;38:27–35. [PubMed: 15061651]
39. Kim JS, Ohshima S, Pediaditakis P, Lemasters JJ. Free Radic. Biol. Med 2004;37:1943–1950. [PubMed: 15544914]
40. Lemasters JJ, Nieminen AL. Biosci. Rep 1997;17:281–291. [PubMed: 9337483]
41. Schnaitman C, Greenawalt JW. J. Cell Biol 1968;38:158–175. [PubMed: 5691970]
42. Becker GL, Fiskum G, Lehninger AL. J Biol. Chem 1980;255:9009–9012. [PubMed: 7410406]
43. Markevich NI, Hoek JB. Computational modeling of ROS production in mitochondria. 2009
44. Hackenbrock CR, Chazotte B, Gupte SS. J Bioenerg. Biomembr 1986;18:331–368. [PubMed: 3021714]
45. Hackenbrock CR. J Cell Biol 1966;30:269–297. [PubMed: 5968972]
46. Hackenbrock CR. J Cell Biol 1968;37:345–369. [PubMed: 5656397]
47. Lemasters JJ. FEBS Lett 1978;88:10–14. [PubMed: 639975]
48. Bielski BH, Cabelli DE. Int. J Radiat. Biol 1991;59:291–319. [PubMed: 1671684]
49. Battistuzzi G, Borsari M, Cowan JA, Eicken C, Loschi L, Sola M. Biochemistry 1999;38:5553–5562. [PubMed: 10220343]
50. Sinibaldi F, Fiorucci L, Patriarca A, Lauceri R, Ferri T, Coletta M, Santucci R. Biochemistry 2008;47:6928–6935. [PubMed: 18540683]
51. Vanlier J, Wu F, Qi F, Vinnakota KC, Han Y, Dash RK, Yang F, Beard DA. Bioinformatics 2009;25:836–837. [PubMed: 19244386]
52. Wu F, Yang F, Vinnakota KC, Beard DA. J. Biol. Chem 2007;282:24525–24537. [PubMed: 17591785]
53. Tan W, Colombini M. Biochim. Biophys. Acta 2007;1768:2510–2515. [PubMed: 17617374]
54. Baines CP, Kaiser RA, Sheiko T, Craigen WJ, Molkentin JD. Nat. Cell Biol 2007;9:550–555. [PubMed: 17417626]
55. Zhao H, Kalivendi S, Zhang H, Joseph J, Nithipatikom K, Vasquez-Vivar J, Kalyanaraman B. Free Radic. Biol. Med 2003;34:1359–1368. [PubMed: 12757846]
56. Georgiou CD, Papapostolou I, Patsoukis N, Tsegenidis T, Sideris T. Anal. Biochem 2005;347:144–151. [PubMed: 16246291]
57. Mukhopadhyay P, Rajesh M, Yoshihiro K, Hasko G, Pacher P. Biochem. Biophys. Res. Commun 2007;358:203–208. [PubMed: 17475217]
58. Baines CP, Kaiser RA, Purcell NH, Blair NS, Osinska H, Hambleton MA, Brunskill EW, Sayen MR, Gottlieb RA, Dorn GW, Robbins J, Molkentin JD. Nature 2005;434:658–662. [PubMed: 15800627]
59. Gincel D, Zaid H, Shoshan-Barmatz V. Biochem. J 2001;358:147–155. [PubMed: 11485562]
60. Battistuzzi G, Borsari M, Cowan JA, Ranieri A, Sola M. J Am Chem. Soc 2002;124:5315–5324. [PubMed: 11996572]
61. Butler J, Jayson GG, Swallow AJ. Biochim. Biophys. Acta 1975;408:215–222. [PubMed: 60]

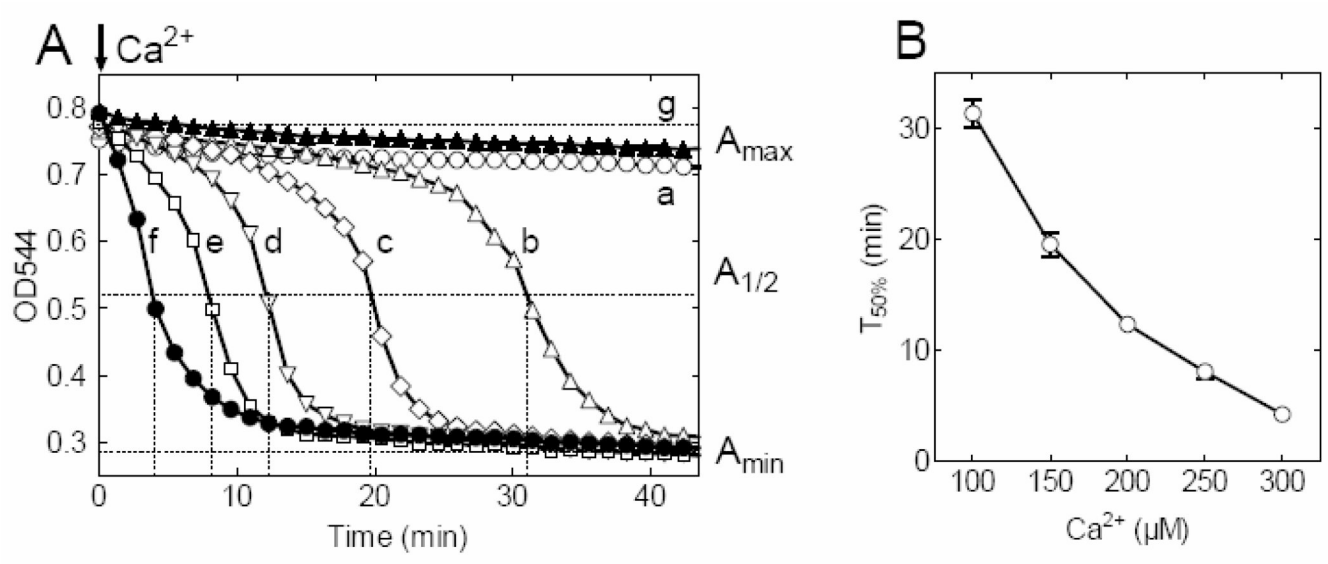

Fig. 1. Increasing Ca^{2+} loading accelerates the occurrence of the MPT in mitochondria

A, Mitochondria (1 mg of protein/ml) were added to incubation buffer containing 200 mM sucrose, 5 mM succinate, 2 μM rotenone, 1 μg/ml oligomycin, 1 mM KH_2PO_4, 20 μM EGTA, 20 mM Tris/HEPES buffer, pH 7.2, and exposed to various concentrations of Ca^{2+} (0, 100, 150, 200, 250, 300 μM, curve **a** through **f**, respectively). Onset of the MPT was monitored by absorbance, as described in **Materials and Methods**. The long horizontal dashed lines mark the levels of the maximal (A_{max}), minimal (A_{min}) and the median ($A_{1/2}$) level of absorbance. Vertical dashed lines mark the time points to 50% MPT for different Ca^{2+} concentrations. As indicated, CsA (1 μM) was added with 300 μM Ca^{2+} (curve **g**, *filled triangles*). *B*, Dependence of onset of MPT on Ca^{2+} concentration. The data shown are representative of at least four independent experiments.

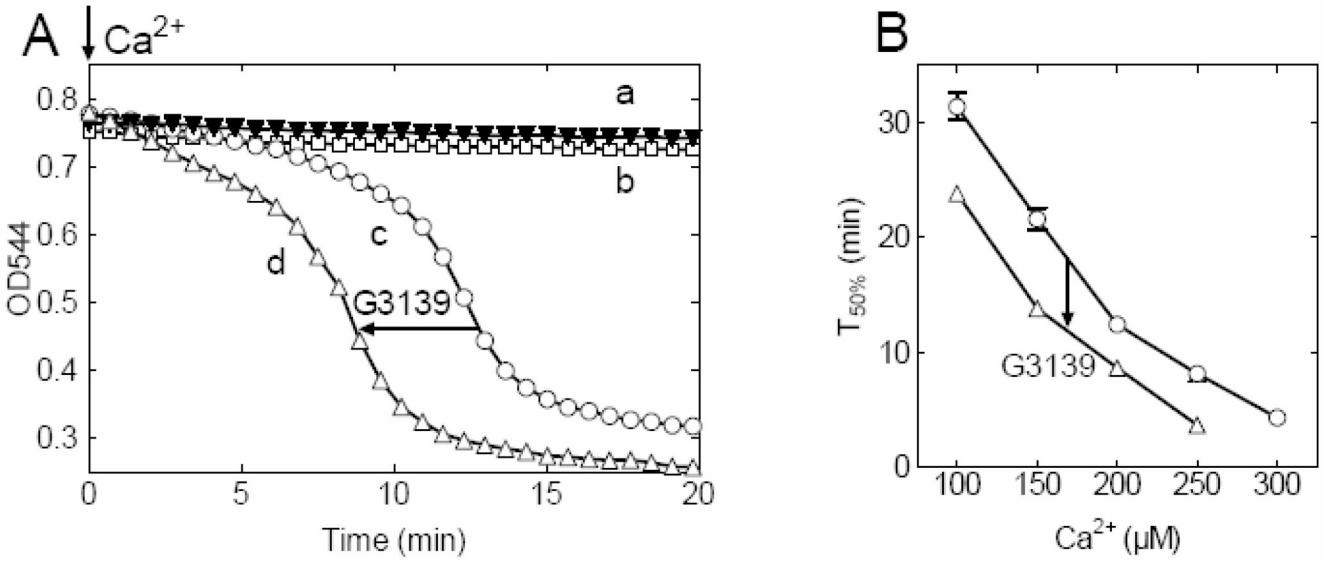

Fig. 2. Closure of VDAC accelerates the occurrence of the Ca^{2+}-induced MPT

A, Onset of 200 μM Ca^{2+}-induced MPT in untreated mitochondria (curve **c**, *open circles*) and mitochondria treated with 5 μM G3139 (curve **d**, *open triangles*). Shown also the changes in the absorbance of mitochondria treated with G3139 in the absence of added Ca^{2+} (curve **b**, *open squares*), and mitochondria treated with CsA and loaded with 200 μM Ca^{2+} (curve **a**, *filled triangles*). *B*, Dependence of the onset of MPT on Ca^{2+} concentrations in control, untreated (*open circles*) and 5 μM G3139-treated (*open triangles*) mitochondria. The data shown are representative of at least four independent experiments, $p<0.05$.

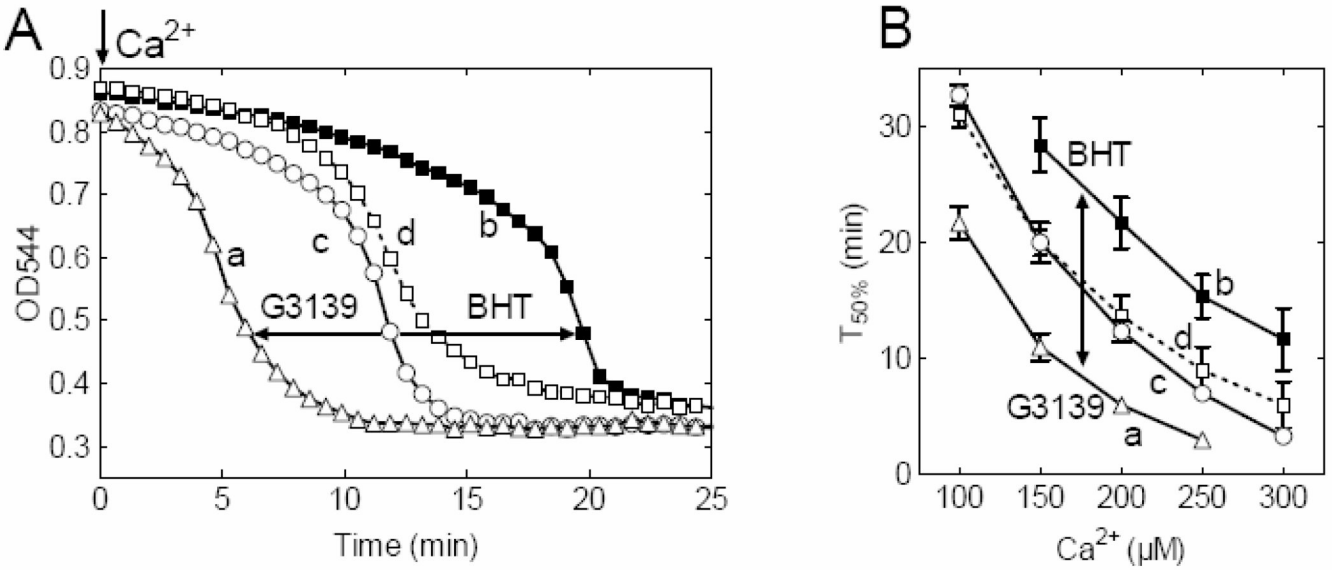

Fig. 3. Butylated hydroxytoluene (BHT) delays MPT occurrence and reverses the effect of G3139

A, Onset of 200 μM Ca^{2+}-induced MPT in mitochondria under different conditions: no treatment (curve **c**, *open circles*), treated with 5 μM G339 (curve **a**, *open triangles*), treated with 20 μM BHT (curve **b**, *filed squares*) and treated with both, 5 μM G3139 and 20 μM BHT (curve d, *open squares*). *B*, Ca^{2+} dose dependence of the onset of MPT in control (*open circles*), G3139 treated (*open triangles*) and BHT treated (*filed squares*) mitochondria. The dotted line (*open squares*) demonstrates the onset of MPT in mitochondria in the presence of both, G3139 and BHT. The data shown are representative of at least four independent experiments, $p<0.05$.

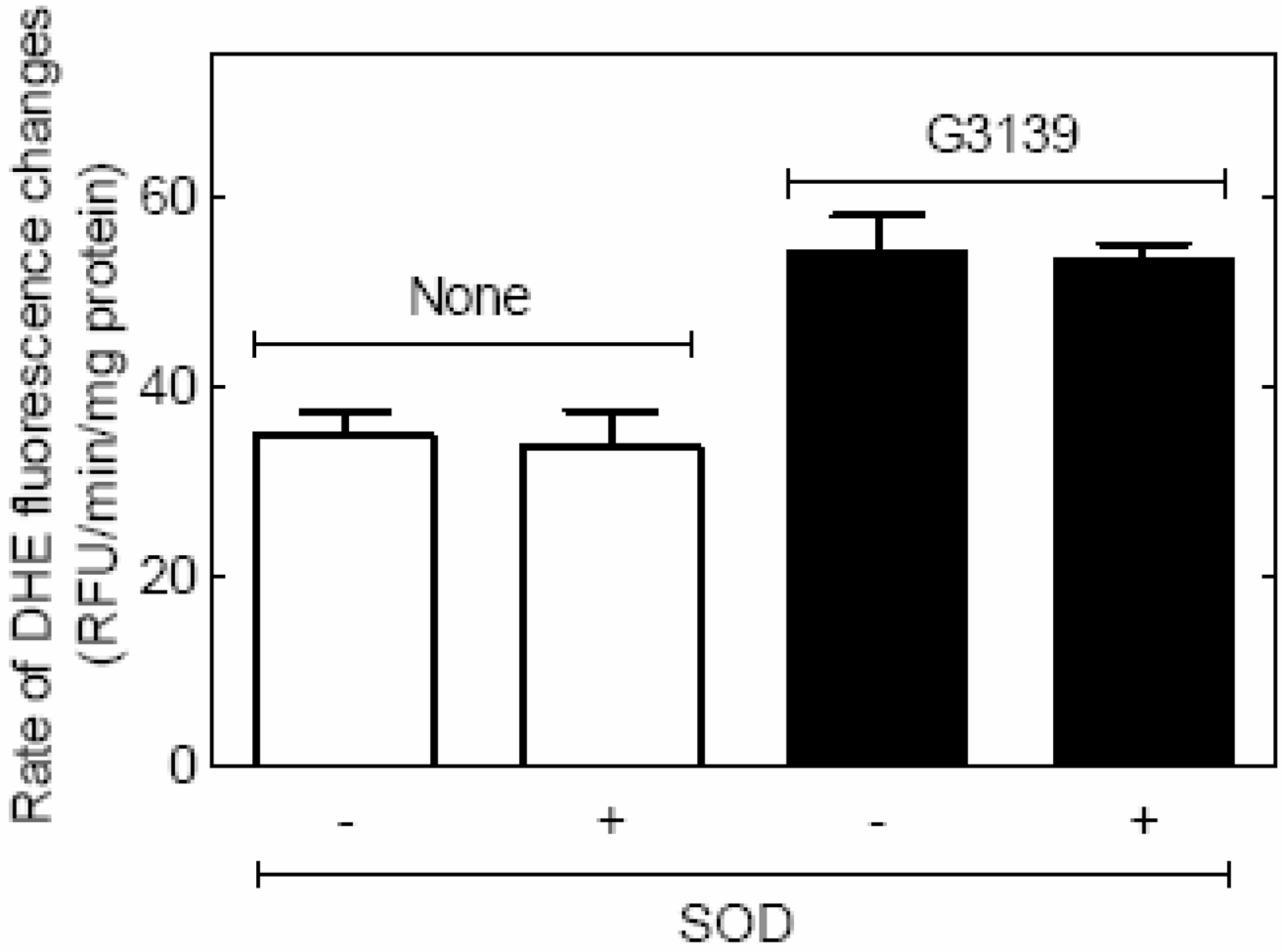

Fig. 4. Closure of VDAC increases the level of superoxide anions in mitochondria

The rates of superoxide production in mitochondria with open (**None**, *open bars*) and closed VDAC (**G13139**, *filled bars*). Mitochondria (1 mg/ml) were incubated in the buffer containing 200 mM sucrose, 5 mM succinate, 2 μM rotenone, 1 μg/ml oligomycin, 1 mM KH_2PO_4, 20 μM EGTA, 20 mM Tris/HEPES, pH 7.4 and was supplemented with antimycin A (1 μg/ml). Shown the level of superoxide in both, control and G3139-treated mitochondria in the absence (− SOD) and presence (+ SOD) of superoxide dismutase. The data shown are representative of at least three independent experiments, $p<0.05$.

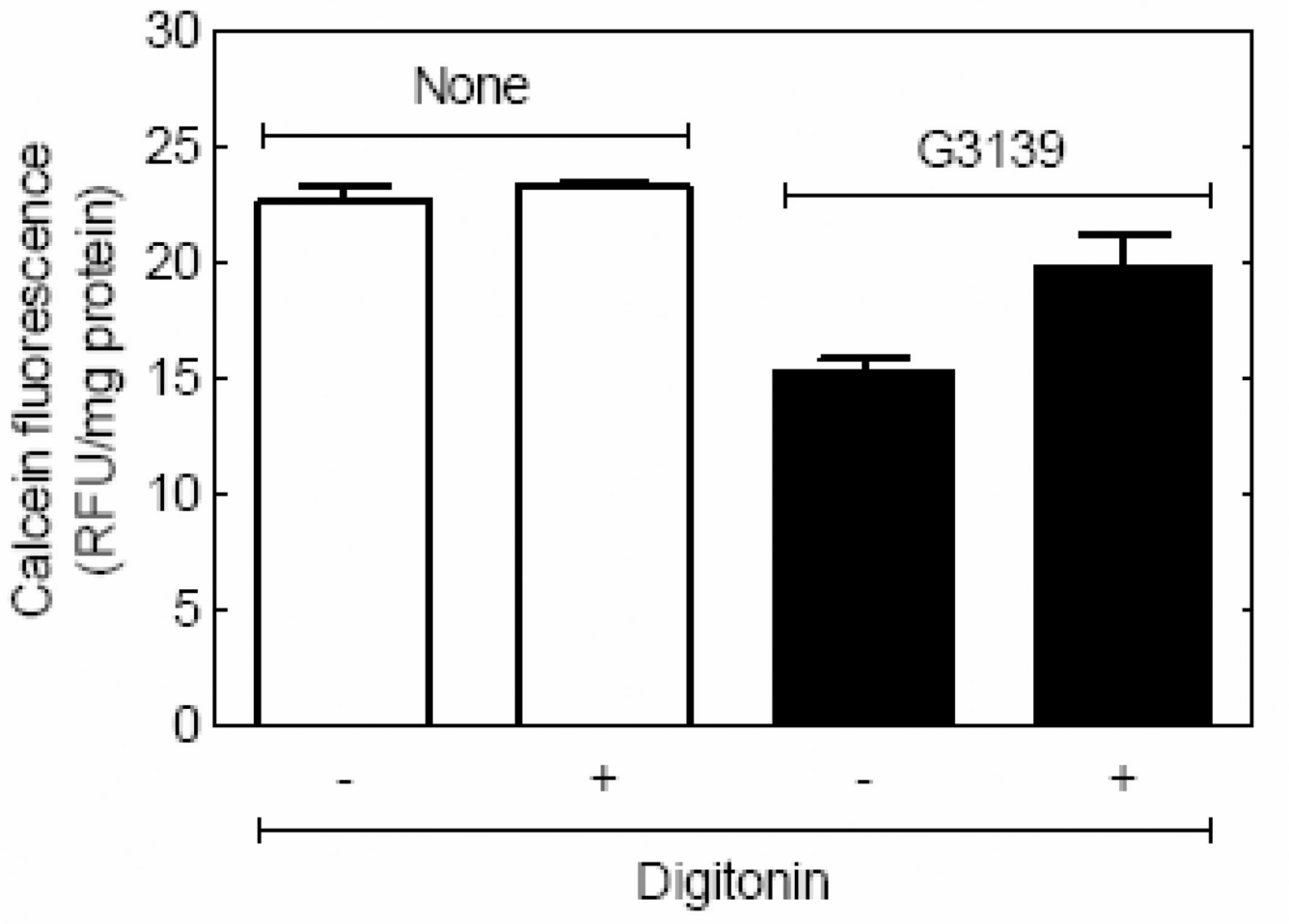

Fig. 5. Closure of VDAC decreases the uptake of Calcein into IMS of mitochondria

Accumulation and retention of VDAC permeating fluorescent molecules of Calcein (MW 622.5) in mitochondria (1 mg/ml) with open (**None**, *open bars*) and closed VDAC (**G3139**, *filled bars*). Mitochondria (1 mg/ml) were incubated in the buffer containing 200 mM sucrose, 5 mM succinate, 2 μM rotenone, 1 μg/ml oligomycin, 1 mM KH_2PO_4, 20 μM EGTA, 20 mM Tris/HEPES, pH 7.4 supplemented with 40 μM of Calcein. Shown are Calcein fluorescence remained with mitochondria following centrifugation of the through the silicone oil (14,000 × g, 60 s) in the absence (− DIG) and presence (+ DIG) of digitonin. The data shown are representative of at least three independent experiments, $p<0.05$.

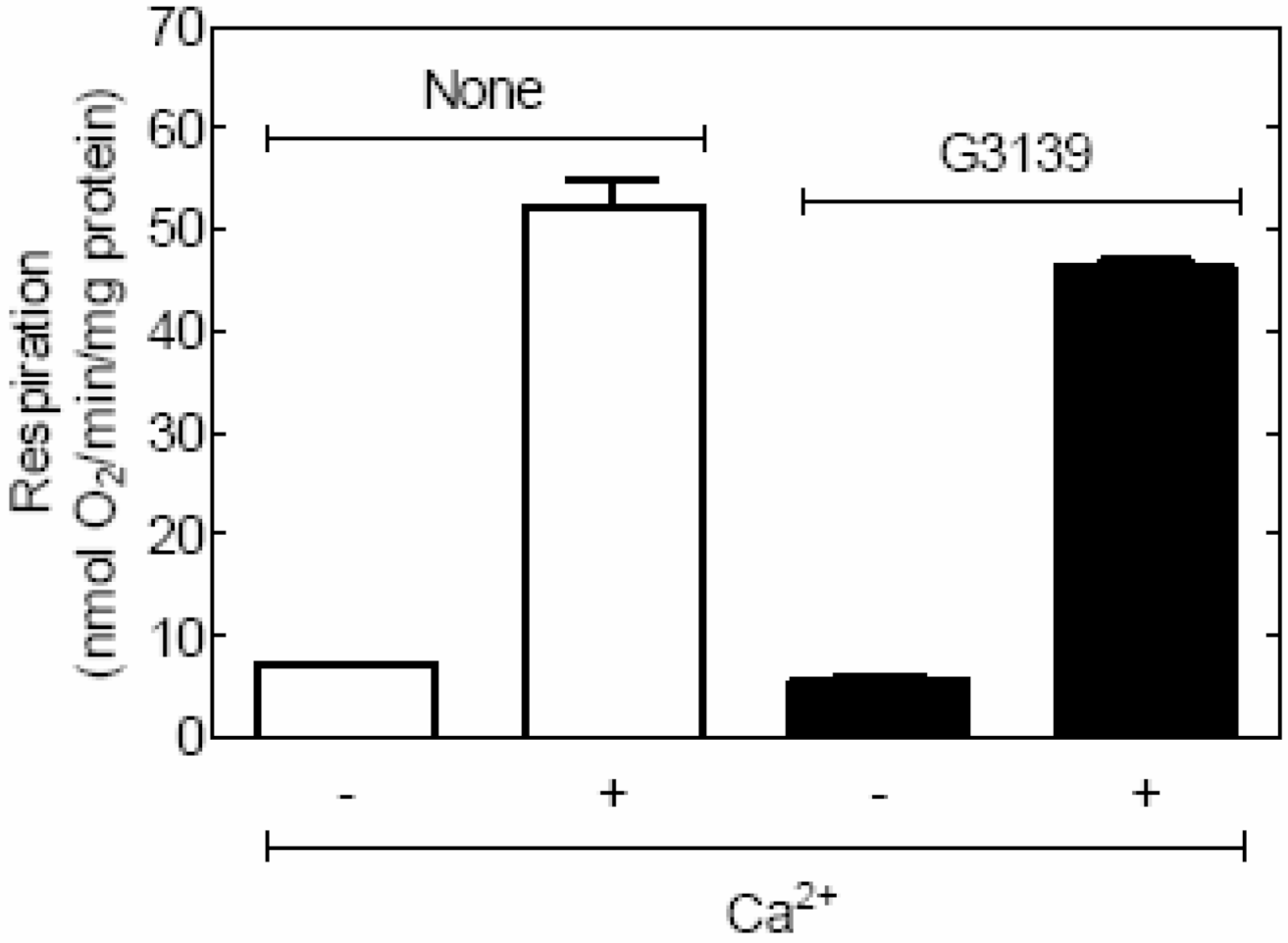

Fig. 6. Closure of VDAC does not decrease Ca^{2+}- uptake in mitochondria

Acceleration of oxygen consumption in mitochondria (1 mg/ml) with open (**None**, *open bars*) and closed VDAC (**G3139**, *filed bars*). Mitochondria (1 mg/ml) were incubated in the buffer containing 200 mM sucrose, 5 mM succinate, 2 μM rotenone, 1 μg/ml oligomycin, 1 mM KH_2PO_4, 20 μM EGTA, 20 mM Tris/HEPES, pH 7.4 and exposed to 250 μM $CaCl_2$. Shown are the respiration of mitochondria in the absence (− Ca^{2+}) and presence (+ Ca^{2+}) of $CaCl_2$. The data shown are representative of at least three independent experiments, $p<0.05$.

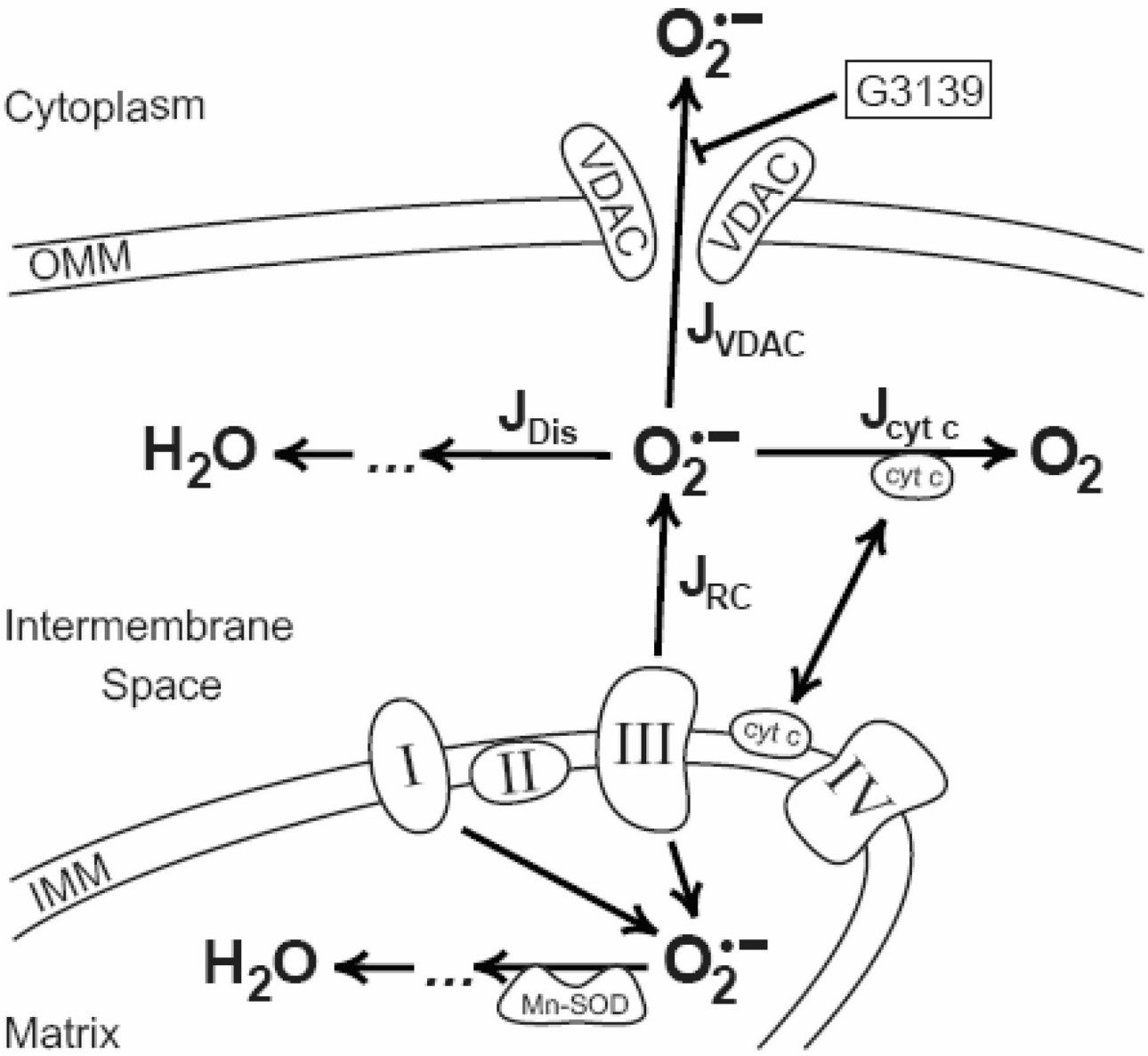

Fig. 7. Simplified diagram of $O_2^{\bullet-}$ generation and utilization within IMS of mitochondria

Complex III of the respiratory chain located within the inner mitochondrial membrane (**IMM**) releases superoxide into the **Matrix** and into the **Intermembrane space**. Matrix superoxide is detoxified by mitochondrial Mn-SOD, and IMS superoxide participates in the reaction of spontaneous dismutation ($\mathbf{J_{Dis}}$), reduction of the cytochrome c ($\mathbf{J_{cyt\ c}}$) and/or leaves IMS ($\mathbf{J_{VDAC}}$) through the open VDAC in the outer mitochondrial membrane (OMM). VDAC blocker (**G3139**) closes VDAC and impedes the efflux of superoxide from IMS. These processes of generation and annihilation of $O_2^{\bullet-}$ within the IMS of mitochondria were used for mathematical modeling of superoxide metabolism in mitochondria.

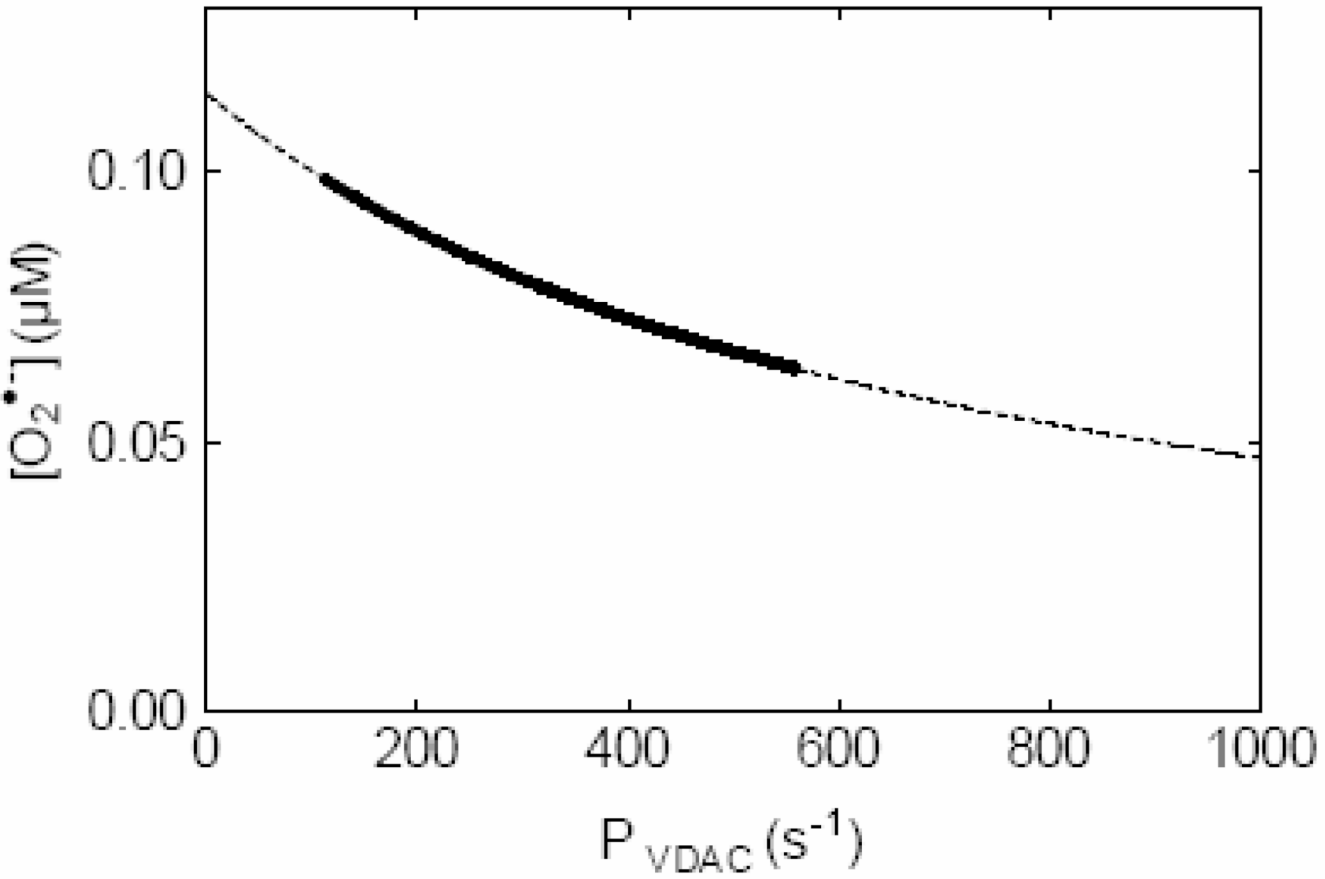

Fig. 8. Predicted steady-state concentration of $O_2^{\bullet-}$ within the IMS as function of open/closed status of VDAC

Computer simulated steady statẽ concentration of $O_2^{\bullet-}$ within IMS upon progressive closure of VDAC (*dotted line*). The range of expected steady state concentrations of $O_2^{\bullet-}$ for permeability of VDAC approximated from available experimental data shown as solid segment of the entire curve. Dotted line also extrapolated to the concentrations of $O_2^{\bullet-}$ within IMS with completely closed VDAC (intersection at $P_{VDAC} = 0$).

Table 1

Parameters of the model

No	Item (constant, flux, etc)	Value (nmoles, s^{-1}, etc)	Source
1	Turnover number for superoxide generation by isolated cytochrome *bc1* complex, k_{bc1}	1 s^{-1} (determined in the presence of Antimycin A)	(3)
2	Concentration of *bc1* complexes per mg of mitochondrial protein	0.041 nmol/mg protein	(44)
3	Volume fraction of mitochondria to IMS (V_{mit})/V_{IMS})	2	(44)
4	Rate constant of spontaneous dismutation (k_{dis})	0.6 $\mu M^{-1}s^{-1}$	(48)
5	Midpoint potential of *cytochrome c*(Fe^{3+})/(Fe^{2+})	+ 260 mV	(49,60)
6	Midpoint potential of $O_2/O_2^{\bullet-}$	− 150 mV	(49,60)
7	The rate constant of cytochrome c oxidation of $O_2^{\bullet-}$ ($k_{cyt\ c}$)	1 $\mu M^{-1}s^{-1}$	(61)